buildings

MDPI

Article

Study on the Properties of Belite Calcium Sulfoaluminate Cement–Ordinary Portland Cement Composite Cementitious System

Xiangyu Xin [1], Guangbin Duan [1,*], Jiang Zhu [2], Pengkun Hou [1], Piqi Zhao [2], Peng Du [2], Shoude Wang [2] and Yongbo Huang [2,*]

[1] School of Materials Science and Engineering, University of Jinan, Jinan 250022, China; mse_xinxy@163.com (X.X.)
[2] Shandong Provincial Key Lab of Preparation and Measurement of Building Materials, University of Jinan, Jinan 250022, China
* Correspondence: mse_duangb@ujn.edu.cn (G.D.); mse_huangyb@ujn.edu.cn (Y.H.)

Abstract: Due to low early strength and high shrinkage, ordinary Portland cement (OPC) has difficulty meeting the actual needs of modern construction projects, while belite calcium sulfoaluminate cement (BCSA–OPC) composite cement provides a new solution. The mechanical and the drying shrinkage properties of the BCSA–OPC mortar were determined, the hydration heat of the BCSA–OPC was studied, and the pore size distribution of the mortar was investigated. In addition, the hydration products of the BCSA–OPC were analyzed by X-ray diffraction (XRD) and simultaneous thermal analysis (TG-DSC), and the microscopic morphology of the BCSA–OPC mortar was observed by scanning electron microscopy (SEM). The results show that with the increase in BCSA dosage in the BCSA–OPC, compared with OPC, the flexural strengths of the mortar of 50% dosage of BCSA at the hydration age of 1 d, 3 d, 7 d, and 28 d are improved by 33.3%, 36.6%, 23.6%, and 26.8%, and the compressive strengths are improved by 50.8%, 35.7%, 13.4%, and 27.7%. The drying shrinkage and total porosity of the mortar at the hydration age of 28 d are reduced by 117.4% and 21.55%, respectively. It is attributed to the filling effect of a large amount of ettringite (AFt) and intertwined with the fibrous C-S-H gel to form a network. This study will provide a theoretical basis for the application of the BCSA–OPC engineering.

Keywords: ordinary Portland cement; belite calcium sulfoaluminate cement; composite cement; composite cementitious system

check for updates

Citation: Xin, X.; Duan, G.; Zhu, J.; Hou, P.; Zhao, P.; Du, P.; Wang, S.; Huang, Y. Study on the Properties of Belite Calcium Sulfoaluminate Cement–Ordinary Portland Cement Composite Cementitious System. *Buildings* **2024**, *14*, 890. https://doi.org/10.3390/buildings14040890

Academic Editor: Samir Chidiac

Received: 8 March 2024
Revised: 20 March 2024
Accepted: 21 March 2024
Published: 26 March 2024

1. Introduction

The ordinary Portland cement (OPC) clinker is mainly composed of tricalcium silicate (C_3S), dicalcium silicate (C_2S), tricalcium aluminate (C_3A), and iron phase (C_4AF). The early-age strength of the OPC depends on the calcium silicate hydrate (C-S-H) gel produced by the hydration of C_3S [1]. The AFt is generated by the hydration of C_3A and C_4AF; however, the AFt in OPC-based material is insufficient to overcome the shrinkage caused by water loss. If the tensile stress caused by the shrinkage exceeds the critical strength, the OPC base will crack, resulting in poor resistance to freezing and erosion [2–4].

To improve the early-age strength and reduce the shrinkage of OPC, it can be modified with calcium sulfoaluminate cement (CSA) [5,6]. CSA is a kind of low-carbon cement [7,8] with calcium sulfoaluminate ($C_4A_3\$$) as the dominant clinker mineral. The CSA can rapidly form a large amount of AFt and alumina gel (AH_3) at the early age of hydration. The CSA has the advantages of fast hardening and early strengthening, low shrinkage, excellent freezing resistance, and great erosion resistance [5]; in addition, the CSA has microexpansion properties [9] and is often used as an expansion agent [10–12].

However, the content of C_2S in CSA clinker is low, which causes a slow growth of the late-age strength [13]. Previous studies have proved [14,15] that in the CSA–OPC composite cementitious system, the CSA can effectively enhance the early-age strength of OPC, while OPC plays an important role in enhancing late-age strength. It should be noted that, when CSA and OPC form a composite cement, the compatibility should be fully considered. Piyush et al. [16] showed that CSA–OPC composite cement has microexpansion properties, but the dosage of CSA should not be higher than 30%; otherwise, the hardened cement paste will undergo overexpansion and cause cracks, which is due to the excessive crystalline stress caused by the hydration product of AFt. In addition, a too-high dosage of CSA may also result in abnormal setting or even affect the development of strength [14,17], which is frequently solved by the retarder [18].

However, the calcination of CSA relies on the high-grade bauxite, resulting in high production costs and limiting the application of CSA. The belite calcium sulfoaluminate cement (BCSA), as an excellent alternative to CSA, can be produced by calcining low-grade aluminum-rich industrial solid wastes such as aluminum tailings, aluminum mine, and fly ash below 1250 °C [19–21], with a much lower production cost and energy consumption.

The clinker mineral compositions of BCSA and CSA are similar, but the mineral content is different [22]. The BCSA has a higher content of C_2S and lower content of $C_4A_3\$$. The BCSA is usually subjected to chemical doping during the calcination process (including B_2O_3, Na_2O, K_2O, BaO, MnO_2, and Cr_2O_3) [23,24], which aims to produce lattice distortion of β-C_2S and activate it to become α-C_2S and α′-C_2S with relatively higher hydration activity [25,26]. The hydration rate of α-C_2S and α′-C_2S is faster than other crystalline C_2S, contributing to a higher degree of hydration.

The C_2S in OPC clinker is mostly β-C_2S [27]; therefore, when BCSA is added to OPC, the amount of C_2S rises and the overall activity is improved. Meanwhile, the $C_4A_3\$$ in BCSA can provide OPC with higher early-age strength and compensated shrinkage. In conclusion, theoretically, the modification of OPC by BCSA is more feasible, and the hydration and properties of the BCSA–OPC composite cement are of great importance.

There are many studies on the CSA–OPC, but few on the BCSA–OPC. The purpose of this study is to use the BCSA to improve the properties of OPC, and to obtain a composite cement with high early-age strength, low shrinkage, and low porosity. Therefore, the setting time, the heat of hydration and the hydration products of the BCSA–OPC, the mechanical properties, the drying shrinkage, and the pore size distribution of the BCSA–OPC mortar were studied. The results can provide a theoretical basis for engineering applications of the BCSA–OPC composite cement in practical engineering.

2. Materials and Methods

2.1. Materials

The cements used in this study are OPC produced by Shandong Cement Group Co., Ltd., (Jinan, China). and BCSA, produced by Hebei Polar Bear Building Materials Co., Ltd., (Tangshan, China). The normalized oxide compositions of OPC and BCSA are given in Table 1. The Rietveld fitting plots of the XRD patterns of OPC and BCSA are shown in Figure 1, and the content of each important component of the cement is given.

Table 1. Oxide compositions of cements (wt.%).

Chemical Analysis	CaO	SiO_2	Al_2O_3	MgO	Fe_2O_3	SO_3	K_2O	Na_2O	etc.
OPC	54.32	24.30	9.71	3.93	3.03	2.69	0.63	0.37	1.02
BCSA	45.59	16.30	15.33	3.98	1.32	15.40	0.47	0.25	1.36

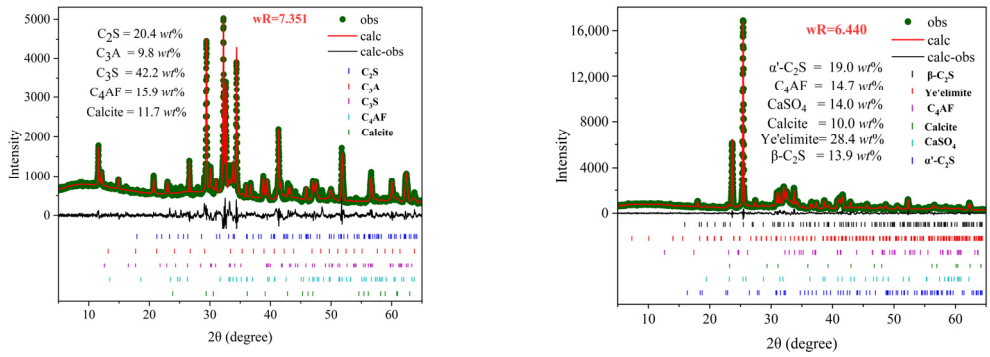

(**a**) (**b**)

Figure 1. Rietveld fitting plots of the XRD patterns: (**a**) OPC; (**b**) BCSA.

2.2. Mixture Proportions and Sample Preparation

The mixing procedure for the BCSA–OPC pastes are shown in Table 2. The mixing procedure for the BCSA–OPC mortars are shown in Table 3.

Table 2. Mix ratio of the BCSA–OPC pastes (wt.%).

Category	B0	B10	B20	B30	B40	B50	B60	B70	B80	B90	B100
BCSA	0	10	20	30	40	50	60	70	80	90	100
OPC	100	90	80	70	60	50	40	30	20	10	0

Table 3. Mix ratio of the BCSA–OPC mortars (g).

Category	OPC	BCSA	Standard Sand	Water
B0	450	0	1350	225
B10	405	45	1350	225
B20	360	90	1350	225
B30	315	135	1350	225
B40	270	180	1350	225
B50	225	225	1350	225

2.3. Methods

2.3.1. Setting Time

The setting time of the cement and the water demand of normal consistency were determined by Vicat apparatus testing according to the Chinese standard GB/T1346-2011 [28]. The paste was mixed with a cement mortar mixer, pouring water and 500 g of cement into the mixing pot and mixing at low speed for 120 s, stopping for 15 s, and then mixing at high speed for 120 s. Finally, it was loaded into molds to test the water demand of normal consistency and the setting time.

The water demand of normal consistency was calculated by Equation (1).

$$P = Mw/M \times 100\% \quad (1)$$

where P is the water demand of normal consistency; Mw is water consumption for mixing, g; and M is the quality of cement, g.

2.3.2. Early Stiffening Test

The early stiffening tests of the cements were determined by Vicat apparatus testing according to the Chinese standard JC/T602-2010 [29]. The mixing time of the cement paste was the same as the Section 2.3.1 setting time. Adopting the cement paste method, the cement was mixed with water according to the water demand of normal consistency, and then the initial needle penetration (I), final needle penetration (F), and remixed needle

penetration (R) of the cement pastes were measured by the Vicat apparatus, respectively. I/F×100% was used to judge the cement solidification.

(1) When the percentage of I/F is ≥50%, it was judged as normal setting.
(2) When the percentage of I/F is <50%, it was considered that the cement was abnormally setting (false set or flash set), so we remixed the paste without adding water, and then measured R. If R < I, the cement was false set, and if R > I, the cement was flash set.

2.3.3. Heat of Hydration

Isothermal calorimeter (TAM Air, Florida, Newcastle, DE, USA) was used to measure the heat release of the cement. A total of 2 g of cement paste in the fresh state was placed into a glass vial (W/C = 0.5). The operating temperature was 20 ± 0.2 °C and the heat flow was recorded every 24 s until 72 h.

2.3.4. XRD Analysis

At the specified hydration age, the hydration of the hardened cement paste was terminated with anhydrous ethanol. Then, the samples were dried at 45 °C for 24 h and grinded with an agate mortar to pass through a 200-mesh sieve. XRD analysis was conducted on a powder diffraction (Rigaku SmartLab, Tokyo, Japan) using Cu Kα radiation (45 kV, 200 mA) with a step size of 0.01° from 5° to 65 °.

To quantify the mineral compositions of OPC and BCSA, Rietveld analysis was conducted on the XRD patterns of cement powders by refining the scale factor, peak asymmetry, zero shift, specimen displacement, and cell parameters.

2.3.5. Mechanical Properties

According to the Chinese standard of GB/T17671-1999 [30], the mortar was 40 mm × 40 mm × 160 mm in size, and there were 3 mortars in each group. A universal testing machine (DYE 300A, Beijing, China) was used to test the flexural strength and the compressive strength of the mortars at the hydration ages of 1 d, 3 d, 7 d, and 28 d. The final results were the average of the strength of mortars in each group.

2.3.6. Drying Shrinkage

The mortar was 25 mm × 25 mm × 280 mm in size, and there were 3 mortars in each group. At the hydration age of 1 d, the mortars were demolded and then placed into the curing box for 2 d, and the initial lengths were recorded using a specific length meter (BC-300, Cangzhou, China). At the drying ages of 1 d, 3 d, 7 d, 14 d, 21 d, and 28 d, the length of mortars was tested and the drying shrinkage was calculated by Equation (2).

$$S_t = (L_0 - L_1)/L \times 100\% \quad (2)$$

where S_t is the drying shrinkage rate of the cement mortar, %; L_0 is the initial reading of the micrometer, mm; L_1 is the average readings in each group at different ages, mm; L is the effective length between the two internal heads of the specimen; 250 mm was taken here.

2.3.7. TG-DSC Analysis

TG-DSC analysis was conducted using a simultaneous thermal analyzer (TA Q600, Florida, Newcastle, DE, USA) from room temperature to 1000 °C under N_2 atmosphere, with a heating rate of 10 °C/min. In total, 20 mg cement pastes with the hydration age of were grinded to pass through a 200-mesh sieve, and were then applied for the TG-DSC analysis.

2.3.8. SEM Analysis

Samples were made of crushed cement mortar at the hydration age of 28 d; the microstructure of samples was observed using an scanning electron microscope (EVO/LS15, Oberkochen, Germany) after sputtering gold coating on the surfaces.

2.3.9. Pore Size Distribution

The mercury intrusion porosimetry (MIP) method was used to obtain the total porosity of the specimens and the proportion of the pores with different sizes. The automatic mercury manometer (AutoPore V 9620, Atlanta, GA, USA) was used to perform mercury-in-pressure tests on the cement mortar specimens with the hydration age of 28 d.

3. Results

3.1. Analysis of Physical and Mechanical Properties of Composite Cement Systems

3.1.1. Setting Time

The water demand for normal consistency and setting time of the BCSA–OPC are shown in Figure 2. The water demand for normal consistency tends to decrease and then increase with the increase in BCSA dosage.

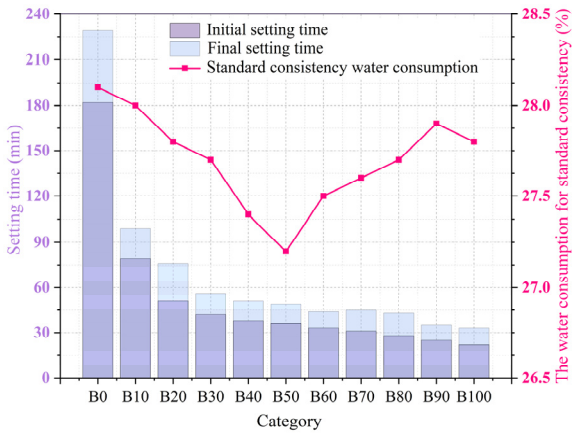

Figure 2. Standard-consistency water consumption and setting time of the BCSA–OPC.

The setting of OPC is due to the continuous nucleation of C-S-H gels produced by the hydration of C_3S and the AFt produced by the hydration of C_3A [31]. The setting of BCSA is due to the hydration of $C_4A_3\$$ to produce AFt. Since the hydration activity of C_3S is lower than that of $C_4A_3\$$ [32], the setting of BCSA–OPC is dominated by $C_4A_3\$$. The setting time decreases with the increase in BCSA dosage. The initial and final setting times of B0 are 182 min and 229 min, respectively. When the dosage of BCSA is 10%, the initial and final setting times are reduced to 79 and 99 min, respectively.

In the cementitious system of the BCSA–OPC, the hydration of $C_4A_3\$$ has an important effect on the setting time. The pH value of the liquid phase of OPC in early-age hydration is significantly higher than that of BCSA [33,34]. The high pH value promotes the hydration of $C_4A_3\$$ to produce the AFt and leads to a decrease in the setting time [5]. The hydration of $C_4A_3\$$ in the general condition is shown in Equation (3), and the hydration of $C_4A_3\$$ in the CH condition is shown in Equation (4). In addition, the AH_3 can react with CH and gypsum to form AFt, and the reaction equation is shown in Equation (5). Therefore, in the existence of CH and gypsum, the hydration production of AFt increases significantly and shortens the setting time of the BCSA–OPC.

$$C_4A_3\$ + 2C\$H_2 + 34H = C_3A{\cdot}3C\${\cdot}32H + 2AH_3 \quad (3)$$

$$C_4A_3\$ + 8C\$H_2 + 6CH + 74H = 3C_3A{\cdot}3C\${\cdot}32H \quad (4)$$

$$AH_3 + 3CH + 3C\$H_2 + 20H = C_3A{\cdot}3C\${\cdot}32H \quad (5)$$

It is recommended that the dosage of BCSA in conventional projects be maintained within 30%, and if there is a need for a higher dosage of BCSA, the retarder is needed.

3.1.2. Early Stiffening Test

The early stiffening test is used to measure the abnormal setting of the cement. The abnormal setting of cement is divided into flash set and false set. The flash set occurs when the cement is exothermic rapidly and hardens when mixed with water. Once water is added and mixed again, its plasticity cannot be restored. On the contrary, the false set occurs when the cement is not exothermic but hardens rapidly when mixed with water. However, if mixed again without adding water, its plasticity can be restored.

In the Portland cement, the abnormal setting has close ties with the formation of large amounts of AFt at the initial hydration age [35]. In the BCSA–OPC composite cementitious system, the hydration of C_3S leads to an increase in pH value, promoting the hydration of $C_4A_3\$$, and the large amount of AFt generation leads to the abnormal setting of BCSA–OPC. Therefore, the study of the abnormal setting of the BCSA–OPC can help to select a reasonable cement mixing ratio and guide the engineering application.

The early stiffening test results of the BCSA–OPC are shown in Figure 3. The initial needle penetration (I) changes are not obvious, while the final needle penetration (F) tends to decrease and then increase, reaching a minimum when the BCSA content is 70%. The flash set of B60, B70, and B80 is due to the mismatch between the amount and activities of gypsum and aluminate minerals in the cement [35,36]. When the C_3A and $C_4A_3\$$ are dissolved into the water and release the Ca^{2+} rapidly into the liquid phase, the small number of negatively charged gypsum particles cannot provide sufficient inhibition, leading to the rapid setting of the cement.

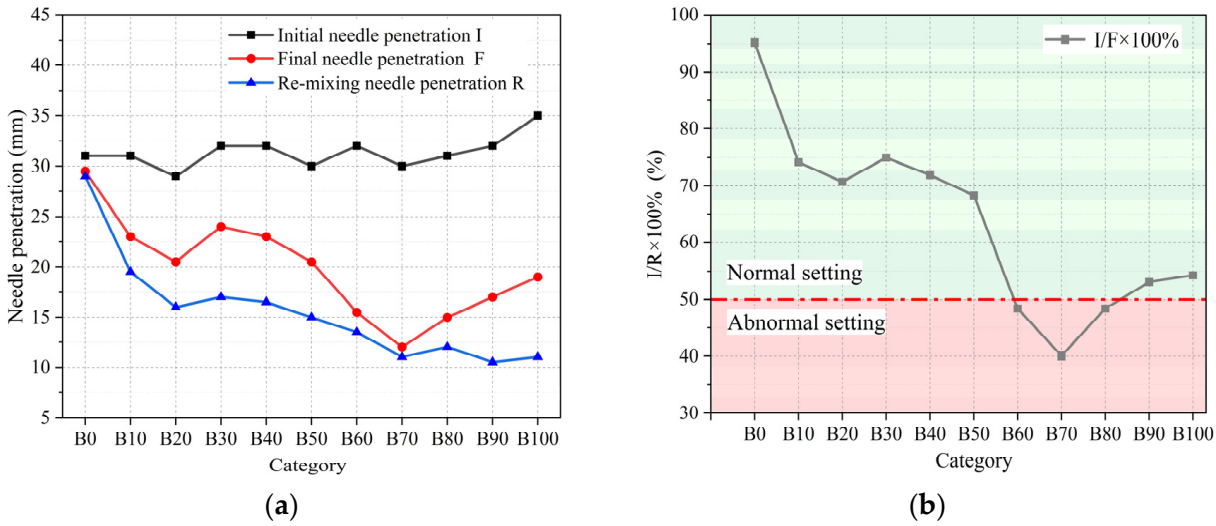

Figure 3. The early stiffening test results of the BCSA–OPC: (**a**) the needle penetration; (**b**) the value of I/R.

The remixing needle penetration (R) is decreased with the increase in BCSA dosage, and the R value of each group is lower than the F value. In summary, except for B60, B70, and B80, other groups showed normal setting. It indicates that when the dosage of BCSA is within the range of 60~80%, the compatibility is not good.

The setting time and the early stiffening test are of great significance in guiding the production of cement and guaranteeing the quality of engineering works [37]. In the BCSA–OPC cementitious system, a high dosage of BCSA leads to a short setting time, and at the dosage of BCSA within 60~80%, the flash set occurs. In addition, the aim of this study is to modify the OPC. Therefore, in the following discussion, B0–B50 will be used to study the hydration and properties of the BCSA–OPC.

3.1.3. Heat of Hydration

Figure 4 shows the cumulative hydration heat and hydration exothermic rate of cements. The cumulative hydration heat reflects the degree of hydration of cement, and the hydration exothermic rate reflects the hydration activity of cement clinker minerals. According to the previous study [38], the early-age strength of cement has a certain correlation with the hydration heat; therefore, the study of the hydration heat is actually studying the early-age strength. The hydration process of OPC is usually divided into four periods: preinduction period, induction period, acceleration period, and delayed period [39]; these characteristics still exist due to the fact that OPC is the main component in B0–B50.

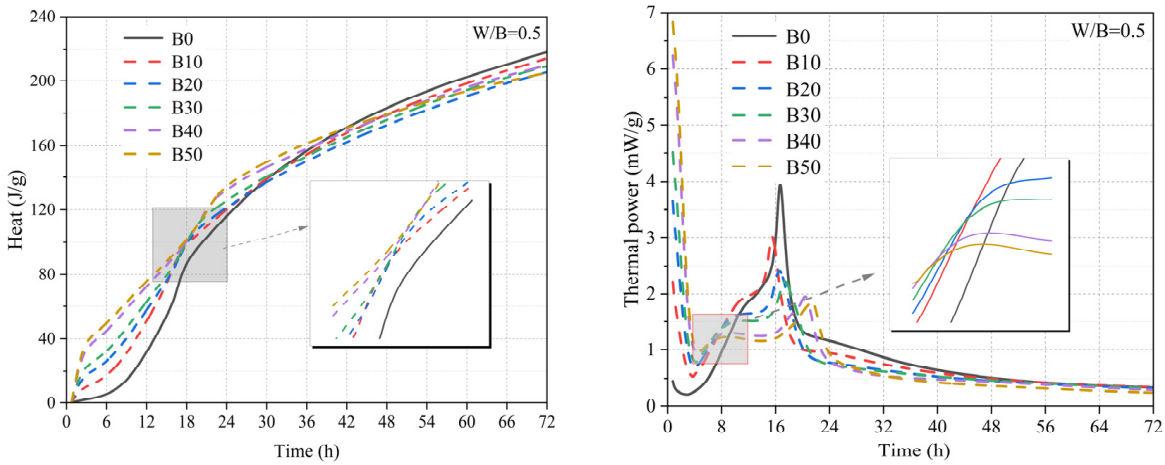

(**a**) (**b**)

Figure 4. The hydration heat of cements: (**a**) the cumulative hydration heat; (**b**) the hydration exothermic rate.

The exotherm of OPC in the preinduction period (0–4 h) was mainly dominated by the hydration of C_3A, while the exotherm of the BCSA–OPC was dominated by $C_4A_3\$$. The exothermic rate of the BCSA–OPC was higher than that of OPC, which is due to the hydration activity of $C_4A_3\$$ being relatively higher than C_3A.

The exotherm of OPC at the induction and acceleration period (4–24 h) was mainly dominated by the hydration of C_3S. The C_3S started to hydrate to produce the C-S-H gel and CH, which increased the pH value of the pore solution [40]. Meanwhile, the hydration of $C_4A_3\$$ in the BCSA–OPC was not finished, and the increase in pH value accelerated the hydration of $C_4A_3\$$. The hydration of $C_4A_3\$$ was almost finished at the hydration time of 8 h. Then, the hydration exothermic rate of the BCSA–OPC started to decrease, and the hydration exothermic rates of B20–B50 were lower than that of OPC, which is related to the decrease in C_3S content. Likewise, the height of the hydration exothermic peak of the BCSA–OPC decreased with the increase in BCSA dosage. Moreover, the increase in BCSA dosage delayed the form of the hydration exothermic peak, which is related to the retardation effect of gypsum in BCSA on C_3S [41].

During the delayed period (24–72 h), the hydration of the remaining C_3S in B0–B50 continued. The hydration exothermic rate decreased with the dosage of BCSA due to the decrease in C_3S content in B0–B50. The hydration exothermic rate decreased slowly with the increase in hydration time.

Compared with OPC, the cumulative hydration heat of BCSA–OPC increased with the increase in BCSA dosage until the hydration time of 30 h. This is attributed to the rapid hydration of $C_4A_3\$$ in the early age of hydration. With the increase in hydration time, the cumulative hydration heat of cements tended to decrease with the increase in BCSA dosage after 40 h. This is because the content of C_3S decreases with the increase in BCSA dosage.

3.1.4. Mechanical Properties

Figure 5 shows the mechanical properties of mortars. The flexural and compressive strengths of the BCSA–OPC at the hydration of all ages tended to increase with the increase in BCSA dosage except for B50 at the hydration of 7 d. Compared with B0, the flexural strengths at the hydration age of 1 d, 3 d, 7 d, and 28 d of B50 were improved by 33.3%, 36.6%, 23.6%, and 26.8%, respectively, and the compressive strengths were improved by 50.8%, 35.7%, 23.4%, and 27.7%, respectively. The compressive strength of B50 was lower than that of B40 at the hydration age of 7 d, but it was still higher than that of B30. This is due to the lower hydration generation of C-S-H gel caused by the lower content of C_3S in B50. The compressive strength of B50 was higher than that of B40 at the hydration age of 28 d. This is attributed to the high C_2S content in B50 and that the activity of C_2S is lower than C_3S.

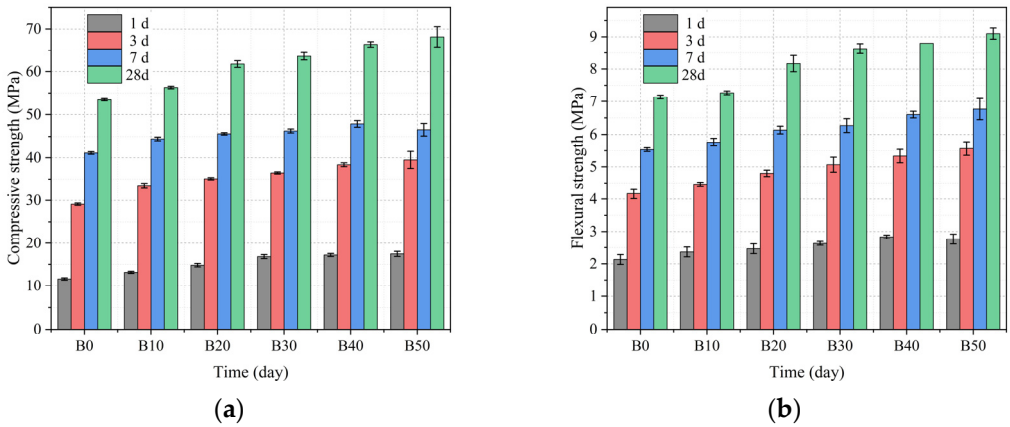

Figure 5. The mechanical properties of mortars: (**a**) compressive; (**b**) flexural.

The early-age strength of the BCSA–OPC was significantly improved compared with OPC. This is attributed to the AFt produced by the hydration of $C_4A_3\$$ [42]. In addition, the CH produced by the hydration of C_3S accelerated the hydration of $C_4A_3\$$, and further increased the hydration production of AFt.

The late-age strength of the BCSA–OPC was also improved. This is attributed to the C_2S in OPC being mostly β-C_2S, but the C_2S in BCSA being mostly α′-C_2S whose hydration activity is higher than β-C_2S. When BCSA was added to OPC, the overall hydration activity of C_2S was improved. A previous study demonstrated that the compressive strength of α′-C_2S was higher than that of β-C_2S at the age of 28 d [43]. Therefore, the late-age strength of the mortar was enhanced with the increase in BCSA dosage.

The mechanical properties of mortar increased with the increase in BCSA dosage at the hydration age of 1 d and 3 d. It is highly correlated with the results of the cumulative hydration heat at the hydration age of 1 d, but contrary to that at the hydration age of 3 d. This is due to the early-age strength of OPC mainly depending on the densification of C-S-H gel hydrated by C_3S [44]. However, the early-age strength of the BCSA–OPC mortar mainly depends on the C-S-H gel growth on the AFt skeleton [45,46]. Therefore, although the cumulative hydration heat decreased with the increase in BCSA dosage at the hydration age of 3 d, the mechanical properties increased.

3.1.5. Drying Shrinkage

The drying shrinkage is important to the cementitious materials. During the hydration process of the cementitious materials, the decrease in absolute volume for the materials leads to the generation of internal tensile stress. When the tensile stress exceeds the tensile strength of the cementitious materials, cracking occurs [47]. The cracks will reduce the durability of the cementitious materials. Figure 6 shows the drying shrinkage of the cement mortars.

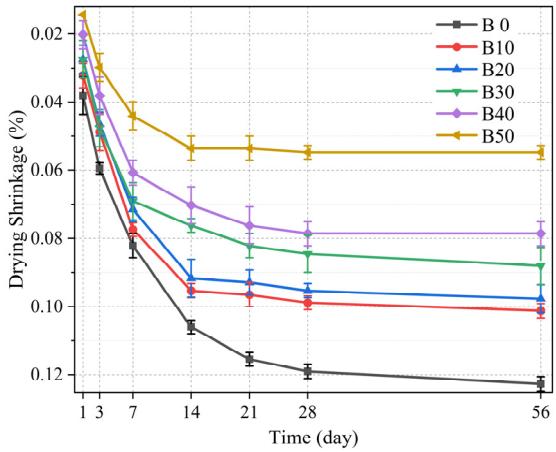

Figure 6. Drying shrinkage of cement mortars.

The results show that the drying shrinkage tended to decrease with the increase in BCSA dosage. The drying shrinkage of B0 was the highest, and B50 was the lowest. The drying shrinkage of each mortar increased rapidly from 1 d to 7 d, which is mainly attributed to the continuous hydration in the early age of the mortar and the massive loss of water in a dry environment. B10–B50 reached a constant value at the hydration age of 14 d, and there was almost no change at the later hydration age, but the drying shrinkage rate of OPC increased continuously. This shows that BCSA could compensate for the drying shrinkage of the BCSA–OPC mortars. Compared with B0, the drying shrinkage at the hydration age 28 d of B10–B50 was reduced by 16.8%, 19.1%, 27%, 36%, and 54%, respectively.

The results show that the drying shrinkage of the BCSA–OPC was significantly lower than that of OPC. This is attributed to the AFt generated by the hydration of $C_4A_3\$$ provided by BCSA. The AFt can improve the density of the mortar and reduce the number of microcracks. Therefore, the drying shrinkage of the mortar is reduced [48].

3.1.6. Pore Size Distribution

Based on the pore size, the pores in cementitious materials are classified into four types [49], which are gel pores below 10 nm, small capillary pores from 10 to 100 nm, large capillary pores from 100 to 1000 nm, and macropores above 1000 nm, among which the pores above 100 nm are the harmful pores. It negatively affects the mechanical properties and impermeability of the mortar. Figure 7 shows the pore structure of mortars at the hydration age of 28 d.

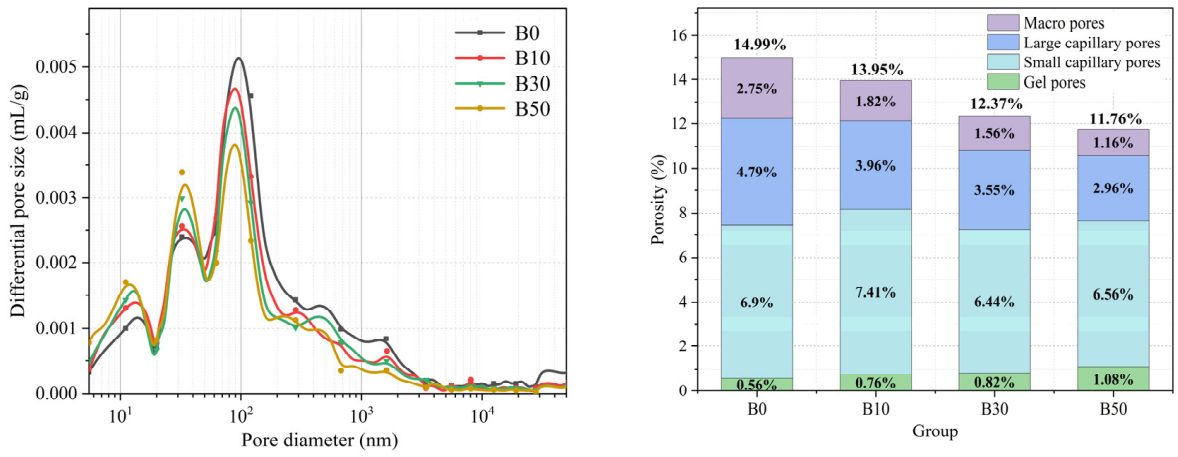

(**a**) (**b**)

Figure 7. The pore structure of mortars: (**a**) the pore size distribution; (**b**) the porosity.

The results show that the total porosity of the mortar decreased with the increase in BCSA dosage. Compared with B0, the total porosity of B50 decreased from 14.99% to 11.76%. With the increase in BCSA dosage, the volume of gel pores increased and the volume of macropores and large capillary pores decreased significantly.

The $C_4A_3\$$ in BCSA can generate a large amount of AFt at the early age of hydration, and a large number of AFt fills the pores of the BCSA–OPC mortars. Therefore, the porosity of the mortar decreased [50,51]. The results indicate that the AFt could reduce the pore sizes of the mortar. The OPC mainly relies on the C-S-H gels generated by hydration to make the internal structure dense, and the C-S-H gels do not have the expansion property [52]; therefore, the total porosity of the BCSA–OPC is lower than that of OPC.

A previous study demonstrated that the early drying shrinkage of mortar is related to the volume of capillary pores [53]. It was also noted that the decrease in the number of large capillary pores and macropores can improve the mechanical properties of the mortar [54]. These studies are consistent with the discussion of mechanical and drying shrinkage properties. Moreover, there are studies that point out that the decrease in porosity also improves resistance to seepage, freezing, and sulfate [55,56].

The physical and mechanical properties of the BCSA–OPC mortars were improved. This is due to the large production of AFt at early-age hydration. The AFt decreases the porosity of the mortars. Meanwhile, the lower porosity helps to reduce the loss of water, and then decreases the drying shrinkage of the mortar [57].

3.2. Compositional and Micromorphological Analysis of Hydration Products

3.2.1. XRD Analysis

Figure 8 shows the XRD patterns of cement pastes at the hydration ages of 1 d, 3 d, 7 d, and 28 d. In the left of each figure are the XRD patterns of the hydration samples, and in the right is the local enlargement of XRD patterns at the range of 32–33°.

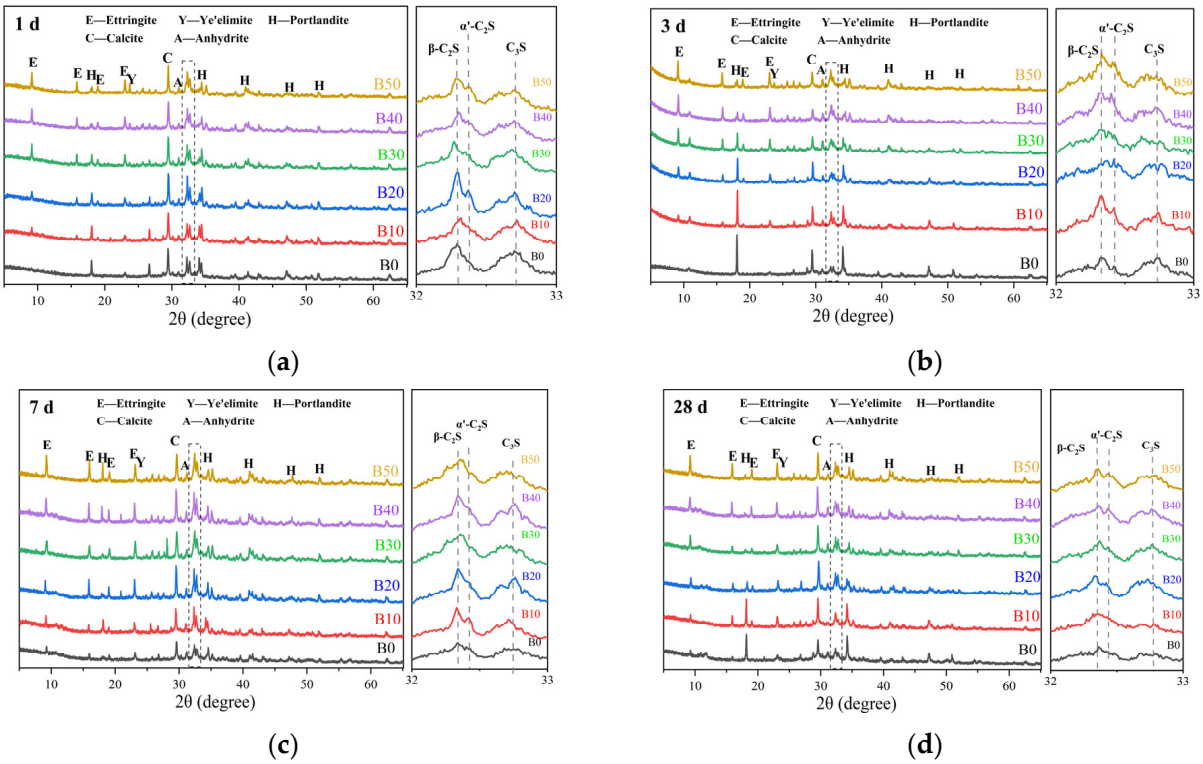

Figure 8. XRD patterns of cement pastes: (**a**) 1 d; (**b**) 3 d; (**c**) 7 d; (**d**) 28 d.

The intensity of the diffraction peaks of ettringite (AFt), ye'elimite ($C_4A_3\$$), and anhydrite (gypsum) increased with the increase in BCSA dosage. Almost all of the $C_4A_3\$$

reacted at the hydration age of 3 d, which played an important role in the increase in AFt and the improvement in the mechanical and drying shrinkage properties, and reduced the porosity of the BCSA–OPC mortar.

The intensities of the diffraction peaks of α′-C_2S and β-C_2S were increased with the increase in BCSA dosage at the hydration ages of 1 d, 3 d, 7 d, and 28 d. The intensity of the diffraction peaks of C_3S decreased with the increase in BCSA dosage at the hydration age of 1 d. Since the $C_4A_3\$$ was fully hydrated at the hydration age of 7 d, it does not contribute to the late-age strength of the BCSA–OPC. Meanwhile, the C_3S is not fully hydrated and the C_2S is just starting to hydrate. The C_3S and C_2S can hydrate to generate the C-S-H gel, which contributes to the late-age strength. This is consistent with the discussion in Section 3.1.4 Mechanical Properties.

The diffraction peaks of anhydrite (gypsum) are still present in all groups at the hydration age 28 d. The gypsum can continuously react with CH and AH_3 to produce AFt. [58], Moreover, the gypsum can prevent the conversion of AFt to AFm. The volume of AFt is larger than that of AFm, which can help to maintain a low porosity and avoid the decrease in the mechanical properties of the mortar in the late age of hydration.

3.2.2. TG–DSC Analysis

Figure 9 shows the TG–DSC curves of the cement pastes at the hydration age of 28 d. The endothermic peaks around 60–170 °C correspond to the decomposition of AFt and C-S-H gel, the endothermic peaks around 170–250 °C correspond to the decomposition of AFm and gypsum, the endothermic peaks around 450–550 °C correspond to the decomposition of CH, and the endothermic peaks around 650–800 °C correspond to the decomposition of $CaCO_3$ [59–61].

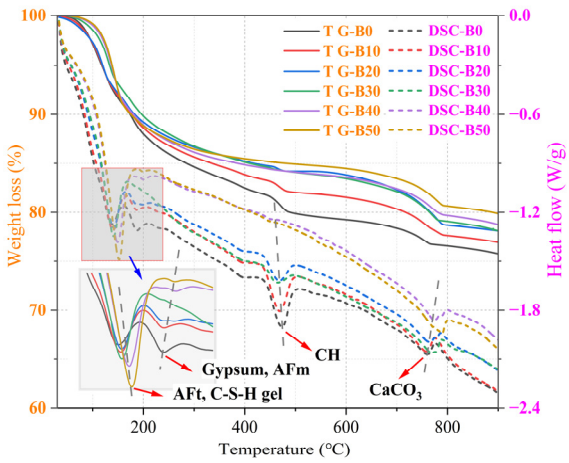

Figure 9. TG–DSC curves of cement pastes.

The results show that the weight loss of AFt and C-S-H gel increased with the dosage of BCSA. The loss of gypsum and AFm decreases with the increase in BCSA dosage, which is due to the sufficient gypsum provided with the BCSA; only when there is insufficient gypsum available is the AFm generated by hydration [62]. It is also understood that AFm can react with SO_4^{2-} to form AFt [63]. The loss of CH decreases with the increase in BCSA dosage, which is not only due to the reaction of AH_3 and gypsum forming AFt with the participation of CH, but also due to the effect of the carbonation reaction to form $CaCO_3$. This is also corresponding to the weight loss of $CaCO_3$ at 650–800 °C.

3.2.3. SEM Analysis

Figure 10 shows the SEM analysis of the mortars at the hydration age of 28 d under the 10,000 times microscope.

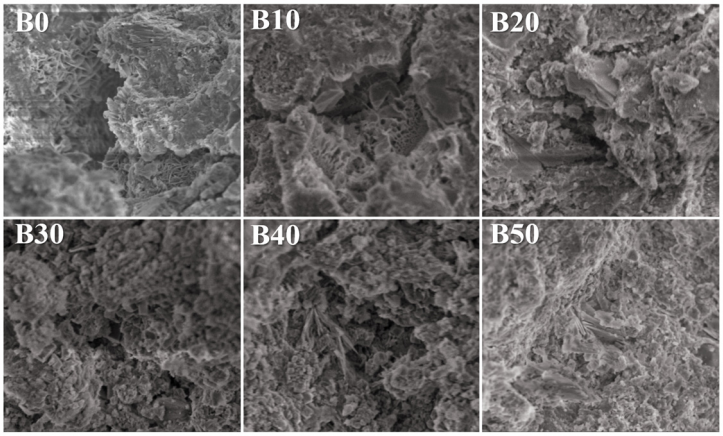

Figure 10. Microscopic morphology of mortars at 10,000×.

The results show that the number of cracks in the BCSA–OPC mortars decreases with the increase in BCSA dosage. This indicates that the BCSA improves the cracking resistance of OPC significantly. This is mainly attributed to the AFt and closely intertwined with the C-S-H gel to form a network structure [64]. This also leads to the improvement in mechanical and drying shrinkage properties as well as the reduction in porosity of the BCSA–OPC mortar. Meanwhile, it was shown that the improvement in cracking resistance contributes to the frost resistance and freezing resistance of the mortar [65].

4. Conclusions

In this study, the hydration mechanism and properties of the BCSA–OPC composite cement were revealed from both macroscopic and microscopic perspectives, and the conclusions are as follows:

(1) The setting time of the BCSA–OPC decreased with the increase in BCSA dosage, and except for BCSA dosage of 60–80%, the rest of the cement could be set normally.
(2) The exothermic rate of hydration of the BCSA–OPC in the preinduction period increased compared with that of OPC, which is due to the increase in $C_4A_3\$$. The exothermic rate of hydration of the BCSA–OPC in the later periods decreased compared with that of OPC, which is due to the decrease in C_3S and the retardation effect of gypsum.
(3) The mechanical properties of the BCSA–OPC mortar increased with the increase in BCSA dosage. Compared with OPC, the flexural strengths at the hydration ages of 1 d, 3 d, 7 d, and 28 d of the BCSA–OPC with 50% BCSA dosage were improved by 33.3%, 36.6%, 23.6%, and 26.8%, respectively, and the compressive strengths were improved by 50.8%, 35.7%, 13.4%, and 27.7%, respectively. This is attributed to the filling effect of a large amount of AFt intertwined with the fibrous C-S-H gel to form a network and make the mortar dense.
(4) The drying shrinkage and total porosity of the BCSA–OPC mortar decreased with the increase in BCSA dosage. The drying shrinkage and total porosity of B50 at the hydration age of 28 d were reduced by 117.4% and 21.55%, respectively. This is due to the fact that AFt has the effect of compensating the shrinkage and blocking the pore size to reduce the water loss.

In conclusion, the properties of the BCSA–OPC were significantly improved compared with OPC. Considering that the cost of BCSA is higher than that of OPC, the dosage of BCSA should be appropriate. Moreover, BCSA has a strong influence on the setting time of OPC; therefore, the dosage of BCSA in normal projects should be strictly controlled to prevent adverse effects on the quality of concrete. When the dosage of BCSA exceeds 30%, it is recommended to use the retarder. In projects with the need for rapid setting, the dosage of BCSA can be increased as appropriate, but should not exceed 50%.

It is believed that this study could provide a significant referential value for engineering applications, and the BCSA–OPC has a wide range of applications. However, the BCSA–OPC may have low alkalinity and this may be not beneficial for its durability. In this study, the long-term mechanical properties and durability of BCSA–OPC were not investigated, which can be the focus of the future research.

Author Contributions: Conceptualization, X.X., G.D. and Y.H.; methodology, X.X.; validation, P.D. and Y.H.; formal analysis, G.D., J.Z. and S.W.; investigation, X.X. and P.H.; data curation, G.D. and P.Z.; writing—original draft preparation, X.X.; writing—review and editing, G.D. and Y.H.; project administration, Y.H.; funding acquisition, Y.H. All authors have read and agreed to the published version of the manuscript.

Funding: This research was funded by Natural Science Foundation of China (52372027, 52002144), Natural Science Foundation of Shandong Province (ZR2020QE046), TaishanScholars Program (tsqnz20221144, tsqn202211170), Science and Technology project of Inner Mongolia Autonomous Region (2022YFHH0118, 2023YFHH0085, 2023YFHH0086). Support Plan for Young Researchers in Institutes of Higher Education in Shandong.

Data Availability Statement: The data presented in this study are available upon request from the corresponding author.

Conflicts of Interest: The authors declare no conflicts of interest.

References

1. Scrivener, K.L.; Nonat, A. Hydration of cementitious materials, present and future. *Cem. Concr. Res.* **2011**, *41*, 651–665. [CrossRef]
2. Yeung, J.S.; Yam, M.C.; Wong, Y.L. Model for predicting shrinkage of concrete using calcium sulfoaluminate cement blended with OPC, PFA and GGBS. *J. Build. Eng.* **2020**, *32*, 101671. [CrossRef]
3. Souza, M.T.; Onghero, L.; Correa, B.N.; Selhorst, M.A.; Dias, A.M.; Repette, W.L.; Pereira, F.R.; Oliveira, A.P.N. Novel low-cost shrinkage-compensating admixture for ordinary Portland cement. *Constr. Build. Mater.* **2020**, *230*, 117024. [CrossRef]
4. Liu, H.; Wang, S.; Huang, Y.; Melugiri, S.B.; Zhang, S.; Cheng, X. Effect of SCMs on the freeze-thaw performance of iron-rich phosphoaluminate cement. *Constr. Build. Mater.* **2020**, *230*, 117012. [CrossRef]
5. Zhang, J.; Li, G.; Ye, W.; Chang, Y.; Liu, Q.; Song, Z. Effects of ordinary Portland cement on the early properties and hydration of calcium sulfoaluminate cement. *Constr. Build. Mater.* **2018**, *186*, 1144–1153. [CrossRef]
6. Li, P.; Gao, X.; Wang, K.; Tam, V.W.Y.; Li, W. Hydration mechanism and early frost resistance of calcium sulfoaluminate cement concrete. *Constr. Build. Mater.* **2020**, *239*, 117862. [CrossRef]
7. Ramanathan, S.; Halee, B.; Suraneni, P. Effect of calcium sulfoaluminate cement prehydration on hydration and strength gain of calcium sulfoaluminate cement-ordinary portland cement mixtures. *Cem. Concr. Compos.* **2020**, *112*, 103694. [CrossRef]
8. Quillin, K. Performance of belite–sulfoaluminate cements. *Cem. Concr. Res.* **2001**, *31*, 1341–1349. [CrossRef]
9. Saoût, G.L.; Lothenbach, B.; Hori, A.; Higuchi, T.; Winnefeld, F. Hydration of Portland cement with additions of calcium sulfoaluminates. *Cem. Concr. Res.* **2013**, *43*, 81–94. [CrossRef]
10. Nagataki, S.; Gomi, H. Expansive admixtures (mainly ettringite). *Cem. Concr. Compos.* **1998**, *20*, 163–170. [CrossRef]
11. Li, C.; Shang, P.; Li, F.; Feng, M.; Zhao, S. Shrinkage and mechanical properties of self-compacting SFRC with calcium-sulfoaluminate expansive agent. *Materials* **2020**, *13*, 588. [CrossRef]
12. Yoo, D.Y.; Kim, S.; Lee, J.Y.; You, I.; Lee, S.J. Implication of calcium sulfoaluminate-based expansive agent on tensile behavior of ultra-high-performance fiber-reinforced concrete. *Constr. Build. Mater.* **2019**, *217*, 679–693. [CrossRef]
13. Pelletier, C.L.; Winnefeld, F.; Lothenbach, B.; Müller, C.J. Beneficial use of limestone filler with calcium sulphoaluminate cement. *Constr. Build. Mater.* **2011**, *26*, 619–627. [CrossRef]
14. Ji, G.; Ali, H.A.; Sun, K.; Xuan, D.; Peng, X.; Li, J. Volume deformation and hydration behavior of ordinary Portland cement/calcium sulfoaluminate cement blends. *Materials* **2023**, *16*, 2652. [CrossRef]
15. Trauchessec, R.; Mechling, J.M.; Lecomte, A.; Roux, A.; Le Rolland, B. Hydration of ordinary Portland cement and calcium sulfoaluminate cement blends. *Cem. Concr. Compos.* **2015**, *56*, 106–114. [CrossRef]
16. Chaunsali, P.; Mondal, P. Influence of calcium sulfoaluminate (CSA) cement content on expansion and hydration behavior of various ordinary Portland cement-CSA blends. *J. Am. Ceram. Soc.* **2015**, *98*, 2167–2624. [CrossRef]
17. Pustovgar, E.; Mishra, R.K.; Palacios, M.; Lacaillerie, J.B.E.; Matschei, T.; Andreev, A.S.; Heinz, H.; Verel, R.; Flatt, R.J. Influence of aluminates on the hydration kinetics of tricalcium silicate. *Cem. Concr. Res.* **2017**, *100*, 245–262. [CrossRef]
18. Pelletier, L.; Winnefeld, F.; Lothenbach, B. The ternary system Portland cement–calcium sulphoaluminate clinker–anhydrite: Hydration mechanism and mortar properties. *Cem. Concr. Compos.* **2010**, *32*, 497–507. [CrossRef]
19. Chen, X.; Li, J.; Lu, Z.; Niu, Y.; Jiang, J.; Xu, Y.; Zhong, W. Preparation and hydration of brownmillerite-belite-sulfoaluminate cement. *Materials* **2022**, *15*, 4344. [CrossRef]

20. Ma, B.; Li, X.; Mao, Y.; Shen, X. Synthesis and characterization of high belite sulfoaluminate cement through rich alumina fly ash and desulfurization gypsum. *Ceram. -Silikáty* **2013**, *57*, 7–13. [CrossRef]
21. Sadananda, S.; Ján, M. Preparation of sulphoaluminate belite cement from fly ash. *Cem. Concr. Res.* **1994**, *24*, 1065–1072. [CrossRef]
22. Rungchet, A.; Poon, C.S.; Chindaprasirt, P.; Pimraksa, K. Synthesis of low-temperature calcium sulfoaluminate-belite cements from industrial wastes and their hydration: Comparative studies between lignite fly ash and bottom ash. *Cem. Concr. Compos.* **2017**, *83*, 10–19. [CrossRef]
23. Koichiro, F.; Ayari, T.; Hideto, Y. Remelting reaction of α-Ca_2SiO_4 solid solution confirmed in Ca_2SiO_4–$Ca_{12}Al_{14}O_{33}$ pseudobinary system. *Cem. Concr. Res.* **2001**, *31*, 1185–1189. [CrossRef]
24. Cuesta, A.; Ayuela, A.; Aranda, M.A.G. Belite cements and their activation. *Cem. Concr. Res.* **2021**, *140*, 106319. [CrossRef]
25. Li, R.; He, W.; Zhang, J.; Wang, Y.; Zhang, Y.; Nie, D. Preparation of belite–sulphoaluminate cement using phosphate rock acid-insoluble residue. *Constr. Build. Mater.* **2022**, *323*, 126573. [CrossRef]
26. Wang, X.; Guo, M.; Yue, G.; Li, Q.; Ling, T. Synthesis of high belite sulfoaluminate cement with high volume of mixed solid wastes. *Soc. Sci. Electron. Publ.* **2022**, *158*, 106845. [CrossRef]
27. Jiang, T.; Cui, K.; Chang, J. Development of low-carbon cement: Carbonation of compounded C_2S by β-C_2S and γ-C_2S. *Cem. Concr. Compos.* **2023**, *139*, 105071. [CrossRef]
28. *GB/T 1346-2011*; Test Methods for Water Requirement of Normal Consistency, Setting Time and Soundness of the Portland Cement. China National Standards Management Committee: Beijing, China, 2011.
29. *JC/T 602-2010*; Test Method for Early Stiffening of Cement. Ministry of Industry and Information Technology of China: Beijing, China, 2010.
30. *GB/T 17671-1999*; Cement Sand Strength Test Method. General Administration Quality Supervision and Quarantine of China: Beijing, China, 1999.
31. Chen, Y.; Odler, I. On the origin of portland cement setting. *Cem. Concr. Res.* **1992**, *22*, 1730–1740. [CrossRef]
32. Phongthorn, J.; Panuwat, J. Utilization of several industrial wastes as raw material for calcium sulfoaluminate cement. *Materials* **2019**, *20*, 3319. [CrossRef]
33. Song, Y.; Zhang, Y.; Shen, S.; Pan, C.; Yan, D.; Wang, Z.; Wang, S.; Ruan, S. Effects of $Ca(OH)_2$ on the reinforcement corrosion of sulfoaluminate cement mortar. *Mater. Struct.* **2023**, *56*, 26. [CrossRef]
34. Encinas, P.; Palomo, A.; Blanco-Varela, M.T.; Fernández-Jiménez, A. Calcium sulfoaluminate clinker hydration at different alkali concentrations. *Cem. Concr. Res.* **2020**, *138*, 106251. [CrossRef]
35. Rakhimbaev, S.M.; Tolypina, N.M.; Anikanova, T.V.M.; Khakhaleva, E.N. Abnormal setting of Portland cement. *J. Phys. Conf. Ser.* **2021**, *1926*, 012066. [CrossRef]
36. Zhang, D. On flash and false setting of cement. *Cement* **2016**, *7*, 17–20. [CrossRef]
37. Kondo, R. False setting of cement. *J. Ceram. Assoc. Jpn.* **1957**, *65*, 211–218. [CrossRef]
38. Li, Z.; Lu, D.; Gao, X. Analysis of correlation between hydration heat release and compressive strength for blended cement pastes. *Constr. Build. Mater.* **2020**, *260*, 120436. [CrossRef]
39. Jansen, D.; Goetz, N.F.; Lothenbach, B.; Neubauer, J. The early hydration of ordinary Portland cement (OPC): An approach comparing measured heat flow with calculated heat flow from QXRD. *Cem. Concr. Res.* **2011**, *42*, 132–138. [CrossRef]
40. Li, Y.; Zhang, H.; Huang, M.; Yin, H.; Jiang, K.; Xiao, K.; Tang, S. Influence of different alkali sulfates on the shrinkage, hydration, pore structure, fractal dimension and microstructure of low-heat Portland cement, medium-heat Portland cement and ordinary Portland cement. *Fractal Fract.* **2021**, *5*, 79. [CrossRef]
41. José, S.A.N.; Erich, D.R.; Monteiro, P.J.M.; Angeles, G.; De, L.T.; Ana, P.K. Hydration of C3S and Al-doped C_3S in the presence of gypsum. *Cem. Concr. Res.* **2022**, *152*, 106686. [CrossRef]
42. Liao, Y.; Yao, J.; Deng, F.; Li, H.; Wang, K.; Tang, S. Hydration behavior and strength development of supersulfated cement prepared by calcined phosphogypsum and slaked lime. *J. Build. Eng.* **2023**, *80*, 108075. [CrossRef]
43. Gies, A.; Knöfel, D. Influence of alkalies on the composition of belite-rich cement clinkers and the technological properties of the resulting cements. *Cem. Concr. Res.* **1986**, *16*, 411–422. [CrossRef]
44. Han, Y.; Xia, J.; Chang, H.; Xu, J. The influence mechanism of ettringite crystals and microstructure characteristics on the strength of calcium-based stabilized soil. *Materials* **2021**, *14*, 1359. [CrossRef] [PubMed]
45. Wu, M.; Zhang, Y.; Jia, Y.; She, W.; Liu, G. Study on the role of activators to the autogenous and drying shrinkage of lime-based low carbon cementitious materials. *J. Clean. Prod.* **2020**, *257*, 120522. [CrossRef]
46. Liu, Z.; Ni, W.; Li, Y.; Ba, H.; Li, N.; Ju, Y.; Zhao, B.; Jia, G.; Hu, W. The mechanism of hydration reaction of granulated blast furnace slag-steel slag-refining slag-desulfurization gypsum-based clinker-free cementitious materials. *J. Build. Eng.* **2021**, *44*, 103289. [CrossRef]
47. Hu, X.; Shi, Z.; Shi, C.; Wu, Z.; Tong, B.; Ou, Z.; Schutter, G. Drying shrinkage and cracking resistance of concrete made with ternary cementitious components. *Constr. Build. Mater.* **2017**, *149*, 406–415. [CrossRef]
48. Cohen, M.; Mobasher, B. Drying shrinkage of expansive cements. *J. Mater. Sci.* **1988**, *23*, 1976–1980. [CrossRef]
49. Ke, G.; Zhang, J.; Liu, Y.; Xie, S. Pore characteristics of calcium sulfoaluminate cement paste with impact of supplementary cementitious materials and water to binder ratio. *Powder Technol.* **2021**, *387*, 146–155. [CrossRef]
50. Yun, H.; Zhang, Y.; Zong, L. The pore structure and hydration performance of sulphoaluminate MDF cement. *J. Wuhan Univ. Technol. Mater. Sci.* **2004**, *19*, 83–85. [CrossRef]

51. Bernardo, G.; Telesca, A.; Valenti, G.L. A porosimetric study of calcium sulfoaluminate cement pastes cured at early ages. *Cem. Concr. Res.* **2006**, *36*, 1042–1047. [CrossRef]
52. Bizzozero, J.; Gosselin, C.; Scrivener, K.L. Expansion mechanisms in calcium aluminate and sulfoaluminate systems with calcium sulfate. *Cem. Concr. Res.* **2014**, *56*, 190–202. [CrossRef]
53. Takahashi, K.; Asamoto, S.; Kobayashi, M.; Bier, T. Effects of fatty alcohol-based shrinkage reducing agents on early-age shrinkage under high temperature conditions. *J. Adv. Concr. Technol.* **2019**, *17*, 648–658. [CrossRef]
54. Wang, S.; Wang, Z.; Huang, T.; Wang, P.; Zhang, G. Mechanical strengths, drying shrinkage and pore structure of cement mortars with hydroxyethyl methyl cellulose. *Constr. Build. Mater.* **2022**, *314*, 125683. [CrossRef]
55. Dong, D.; Huang, Y.; Gao, X. Effect of polyvinyl alcohol powder on the impermeability, frost resistance and pore structure of calcium sulfoaluminate cement concrete. *Constr. Build. Mater.* **2023**, *409*, 133858. [CrossRef]
56. Deng, G.; He, Y.; Lu, L.; Wang, F.; Fu, S. Pore structure evolution and sulfate attack of high-volume slag blended mortars under standard curing and steam curing. *Constr. Build. Mater.* **2023**, *363*, 129878. [CrossRef]
57. Zhang, J.; Ye, C.; Tan, H.; Liu, X. Potential application of Portland cement-sulfoaluminate cement system in precast concrete cured under ambient temperature. *Constr. Build. Mater.* **2020**, *251*, 118869. [CrossRef]
58. Li, X.; Liu, S.; Zhang, H.; Li, H.; Guan, X. Effects of AH_3 and AFt on the hydration–hardening properties of the C_4A_3S-CS-H_2O system. *Materials* **2023**, *16*, 6322. [CrossRef] [PubMed]
59. Zhang, Z.; Du, J.; Shi, M. Quantitative analysis of the calcium hydroxide content of EVA-modified cement paste based on TG-DSC in a dual atmosphere. *Materials* **2022**, *15*, 2660. [CrossRef] [PubMed]
60. Wang, L.; Ju, S.; Chu, H.; Liu, Z.; Yang, Z.; Wang, F.; Jiang, J. Hydration process and microstructure evolution of low exothermic concrete produced with urea. *Constr. Build. Mater.* **2020**, *248*, 118640. [CrossRef]
61. Sun, H.; Qian, J.; Peng, S.; Xiong, M.; Fan, C.; Fan, Y. Utilization of circulating fluidized bed combustion ash to prepare supersulfated cement. *Constr. Build. Mater.* **2022**, *318*, 125861. [CrossRef]
62. Zhang, Y.; Chang, J.; Ji, J. AH_3 phase in the hydration product system of AFt-AFm-AH_3 in calcium sulfoaluminate cements: A microstructural study. *Constr. Build. Mater.* **2018**, *167*, 587–596. [CrossRef]
63. Yu, L.; Chu, H.; Zhu, Z.; Jiang, L.; Dong, H. Determination of the chloride ion content in concrete under simultaneous chloride and sulphate ion attack. *J. Build. Eng.* **2023**, *72*, 106579. [CrossRef]
64. Niu, F.; An, Y.; Zhang, J.; Chen, W.; He, S. Synergistic excitation mechanism of CaO-SiO_2-Al_2O_3-SO_3 quaternary active cementitious system. *Front. Mater.* **2021**, *8*, 792682. [CrossRef]
65. Shen, D.; Liu, K.; Wen, C.; Shen, Y.; Jiang, G. Early-age cracking resistance of ground granulated blast furnace slag concrete. *Constr. Build. Mater.* **2019**, *222*, 278–287. [CrossRef]